On information metrics for spatial coding

Bryan C. Souza[1*,§], Rodrigo Pavão[1,2,§], Hindiael Belchior[3], Adriano B.L. Tort[1]

[1] Brain Institute, Federal University of Rio Grande do Norte, RN, Brazil
[2] Department of Neuroscience, Albert Einstein College of Medicine, NY, USA
[3] Faculty of Health Sciences of Trairi, Federal University of Rio Grande do Norte, RN, Brazil
[§] Equal contribution.
* Correspondence to: bryancsouza@neuro.ufrn.br (BCS)

Abstract

The hippocampal formation is involved in navigation, and its neuronal activity exhibits a variety of spatial correlates (e.g., place cells, grid cells). The quantification of the information encoded by spikes has been standard procedure to identify which cells have spatial correlates. For place cells, most of the established metrics derive from Shannon's mutual information (Shannon, 1948), and convey information in bits/sec or bits/spike (Skaggs et al., 1993; Skaggs et al., 1996). Despite their widespread use, the performance of these metrics in relation to the original mutual information metric has never been investigated. In this work, using simulated and real data, we find that the current spatial information metrics correlate less with the true information content in the data than the original mutual information metric. We propose corrections that yield more accurate and comparable spatial information estimates.

Keywords

Place cell; place field; spatial coding; information; entropy; spike train analysis; hippocampus.

Introduction

The hippocampus is known to be involved in memory formation (Eichenbaum, 2000; Scoville and Milner, 1957) and spatial navigation (Morris et al., 1982; O'Keefe and Dostrovsky, 1971; O'Keefe and Recce, 1993; Zola-Morgan and Squire, 1990). In the early 70s, O'Keefe and Dostrovsky discovered that some hippocampal cells have firing rate modulated by the animal's position, discharging more at a spatial region known as the place field of the cell (O'Keefe and Dostrovsky, 1971). These place cells were later found to relate to the theta rhythm, a prominent hippocampal oscillation present during locomotion and REM sleep (Vanderwolf, 1969). Namely, their spike times couple to theta, and their preferred phase progressively advances from the theta peak as the animal traverses the place field, a phenomenon called phase precession (Huxter et al., 2003; O'Keefe and Recce, 1993; Souza and Tort, 2017).

Since the discovery of place cells, other types of spatial correlates emerged in related areas to the hippocampal circuitry, such as the head-direction cells in the postsubiculum (Taube et al., 1990), and the grid cells and speed cells in the entorhinal cortex (Fyhn et al., 2004; Hafting et al., 2005; Kropff et al., 2015; Moser et al., 2008). Properly identifying these cells requires estimates of the information contained in spikes about navigational features (i.e. position, speed, head angle). The main metrics used to estimate this type of information were proposed by Skaggs et al. (1993, 1996) and are adaptations of Shannon's mutual information (MI).

Information entropy, as originally proposed by Shannon, measures the amount of uncertainty in the outcome of a variable based on its probability of occurrence (Shannon, 1948). In other words, the more unpredictable the outcome is, the more entropy it has. On the other hand, the MI is a measure of the shared entropy between two variables; it indicates how much knowing a variable X reduces the uncertainty of a variable Y. While the MI is usually measured in bits, the two alternative metrics proposed by Skaggs et al. normalize information in such a way as to express it as bits per spike (I_{spike}) or bits per second (I_{sec}). Although these metrics provide a meaningful interpretation of the relation between firing rate and navigational features, which led to their widespread use, the possible caveats introduced by these modifications were never investigated.

In this work, we use simulated data to address how well the metrics I_{spike}, I_{sec} and MI reflect the capacity of decoding the animal's position based on the spikes of an individual neuron, which directly relates to the amount of spatial information conveyed by the cell (Quian Quiroga and Panzeri, 2009). We find that while MI values correlate well with decoding performance under a variety of scenarios, this is not always the case for I_{spike} and I_{sec}. Similar results hold when analyzing real spikes from place cells of rats recorded on a linear track. Finally, we propose a correction based on surrogate analysis that can equalize the three metrics.

Methods

Simulating spatially modulated cells

We simulated the firing rate of spatially modulated neurons across 30 trials on a linear track divided into 25 bins of space (Figure 1A). For simplicity, the animal speed and occupancy were considered constant over space. We modeled eight types of cells; for each cell type, we simulated 10 levels of spatial modulation (Figure 1B, Neuron ID a to j). For the first 5 cell types (Neuronal type I to V), the firing rate of each trial was modeled as a Gaussian centered (on average) at bin 13 with (average) standard deviation of 5 bins. To introduce inter-trial variability, 0.5 and 0.1 white noise was added to the center and standard deviation of the Gaussian, respectively. The cell types mimicked the behavior of (I) a pyramidal-like place cell (low basal firing rate); (II) an interneuron-like place cell (high basal firing rate); (III) interneuron-like place cell negatively modulated by space; (IV) a pyramidal-like place cell exhibiting spatial modulation in a subset of trials; and (V) a cell as in IV, but with constant mean firing rate across trials. For cell types I-III, we varied spatial modulation strength (deviation from baseline), while for cell types IV and V the number

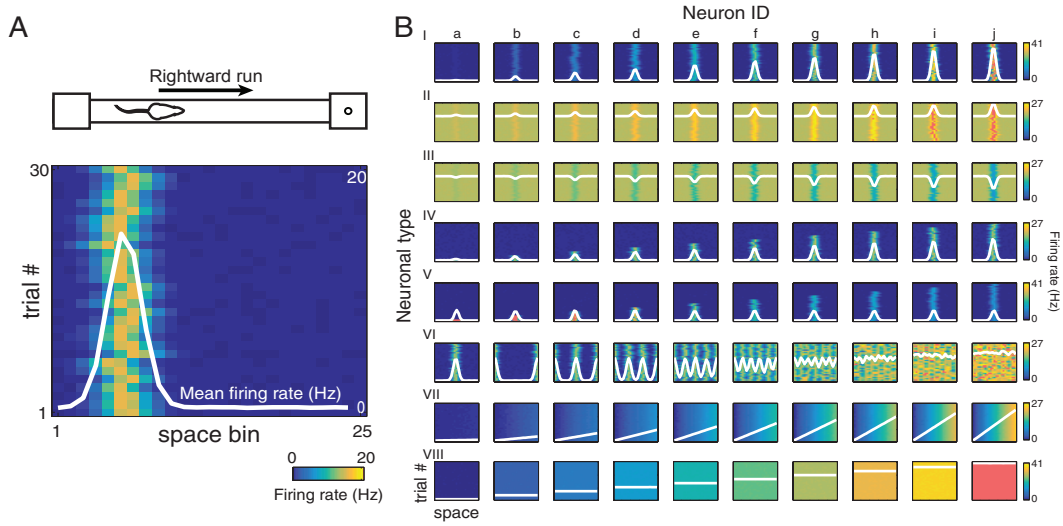

Figure 1. Simulating the activity of spatially modulated neurons. A. Neuronal firing rate was simulated in 25 bins of space over 30 trials, meant to represent spiking activity of one cell during rightward runs on a linear track. In the rate-position map, pseudo-colors represent firing rate on each trial, while the white line is the mean firing rate over trials. **B.** Rows display 8 simulated neuronal types (I-VIII) of different spatial modulation profiles. Cell types I-V exhibit place-cell-like behavior, while types VI, VII and VIII represent grid cells, ramp and constant functions, respectively (see Methods for details). For each type, columns show the rate-position maps (pseudo-color scale) as well as the mean firing rate (overlaying white trace) for 10 distinct cells (a-j) differing in the level of spatial modulation.

of modulated trials varied. Cell type VI was similar to cell type I but could have multiple, equally-spaced peaks as a grid cell. We also simulated cells behaving as ramp (VII) or constant functions (VIII) along space, with different slopes and firing rate levels, respectively.

Estimating spatial information in the firing rate

To estimate the spatial information contained in the firing rate of each cell we used I_{spike} and I_{sec} – the standard approaches used for selecting place cells (Skaggs et al., 1996, 1993) – and the MI (Shannon, 1948). We computed the I_{sec} metric from the average firing rate (over trials) in the 25 space bins using the following definition:

$$I_{sec} = \sum_{i=1}^{25} p_i \lambda_i log_2 \frac{\lambda_i}{\lambda}$$

where λ_i is the mean firing rate in the i-th space bin and p_i the occupancy ratio of the bin, while λ is the overall mean firing rate of the cell.

The I_{spike} metric is a normalization of I_{sec}, defined as:

$$I_{spike} = \frac{I_{sec}}{\lambda}$$

This normalization yields values in bits per spike, while I_{sec} is in bits per second.

The MI was estimated using all firing rate values, which were binned into four non-overlapping quantiles:

$$MI = \sum_{i=1}^{25} \sum_{j=1}^{4} p_{i,j} log_2 \left(\frac{p_{i,j}}{p_i \cdot p_j} \right)$$

where p_i and p_j are the probabilities of position bin i and firing rate bin j, respectively. p_{ij} is the joint probability between position bin i and firing rate bin j.

Estimating spatial information from decoding performance

Decoding algorithms predict the most likely stimulus that generated a given response based on the previous observations of stimulus-response pairs (Quian Quiroga and Panzeri, 2009). We used a naïve Bayes classifier to predict the position of the animal based on the firing rate of a cell. For each cell, the firing rate values (trials x space bins) were used to train and test the decoder in a leave-one-out approach (Figure 2). We then computed the confusion matrix for the actual and decoded positions, and extracted the percentage of correct decoding. The percentage of correct decoding of the classifier was assumed to correlate with the true spatial information content of the cell, and was compared to the outcome of each of the three metrics of spatial information defined above (Figure 3).

Normalizing spatial information metrics using surrogates

To correct the estimates of spatial information, we first shuffled the position of firing rates on each trial (Figure 4A). This approach avoids any firing preference across trials and in the mean rate. We then computed the I_{spike}, I_{sec} and MI metrics using the shuffled rates. This procedure was repeated 100 times and used to build a surrogate distribution for each metric. The information values were then corrected by expressing them as z-scores of the surrogate distribution. The corrected information metrics are referred to as normalized I_{spike} (Norm. I_{spike}), I_{sec} (Norm. I_{sec}) and MI (Norm. MI).

Measuring the spatial information of real place cells

To investigate the relation between the spatial information estimates and decoding performance for real neurons, we used a dataset with recordings from the CA1 region of the dorsal hippocampus of three rats running back and forth on a linear track (Mizuseki et al., 2013;

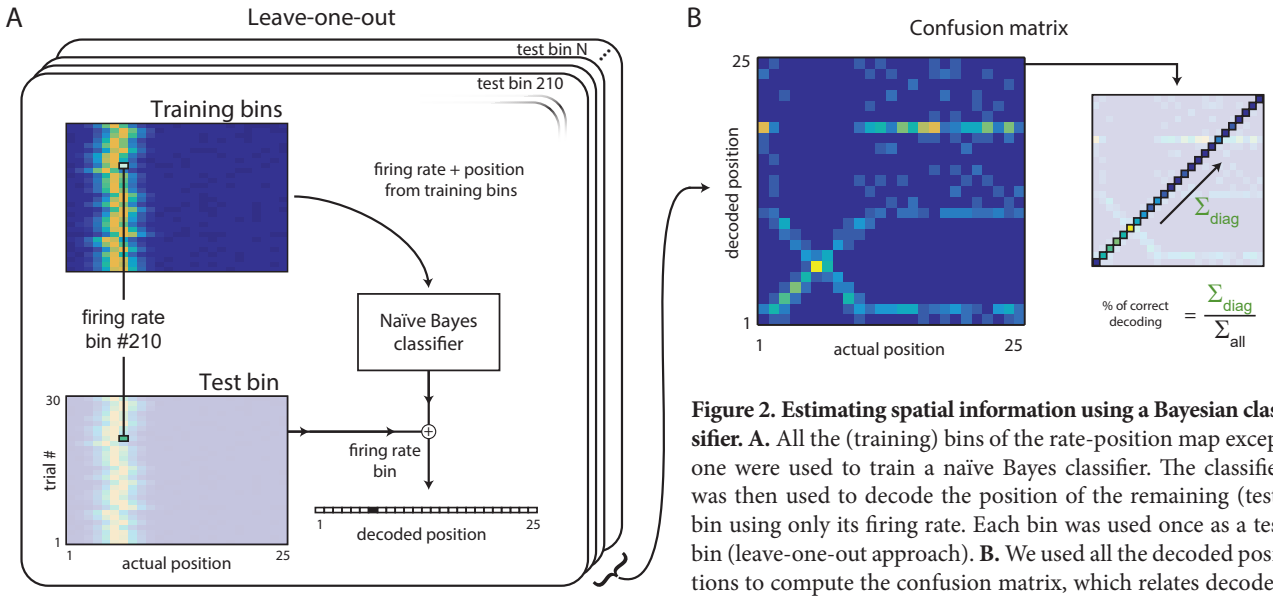

Figure 2. Estimating spatial information using a Bayesian classifier. A. All the (training) bins of the rate-position map except one were used to train a naïve Bayes classifier. The classifier was then used to decode the position of the remaining (test) bin using only its firing rate. Each bin was used once as a test bin (leave-one-out approach). **B.** We used all the decoded positions to compute the confusion matrix, which relates decoded and actual positions. We divided the amount of times the classifier was correct (sum of the matrix diagonal) by the total number of classifications to calculate the decoding performance.

data freely available at https://crcns.org/). We calculated the spatial information estimates and the decoding performance for all neurons in 75 recording sessions.

Results

We first computed the three spatial metrics for each of the 8 simulated cell types shown in Figure 1. These cell types vary in how their firing rate is modulated by space (see Methods). For instance, while cell type I fires at its place field location on every trial, cell type IV emits spatially modulated spikes only in a subset of trials. For each cell type, we varied the amount of spatial modulation in 10 levels. This was achieved by either changing the deviation of the firing rate from the basal level (cell types I-III), or the percentage of trials with modulated activity (cell types IV and V), number of place fields (cell type VI), spatial slope (cell type VII) or basal firing rate level (cell type VIII). The spatial metrics were then compared with the percentage of correct decoding of a Bayesian classifier.

Figure 3A,B shows examples in which the same decoding performance could have either high or low values of I_{sec} and I_{spike} (compare different rows in Figure

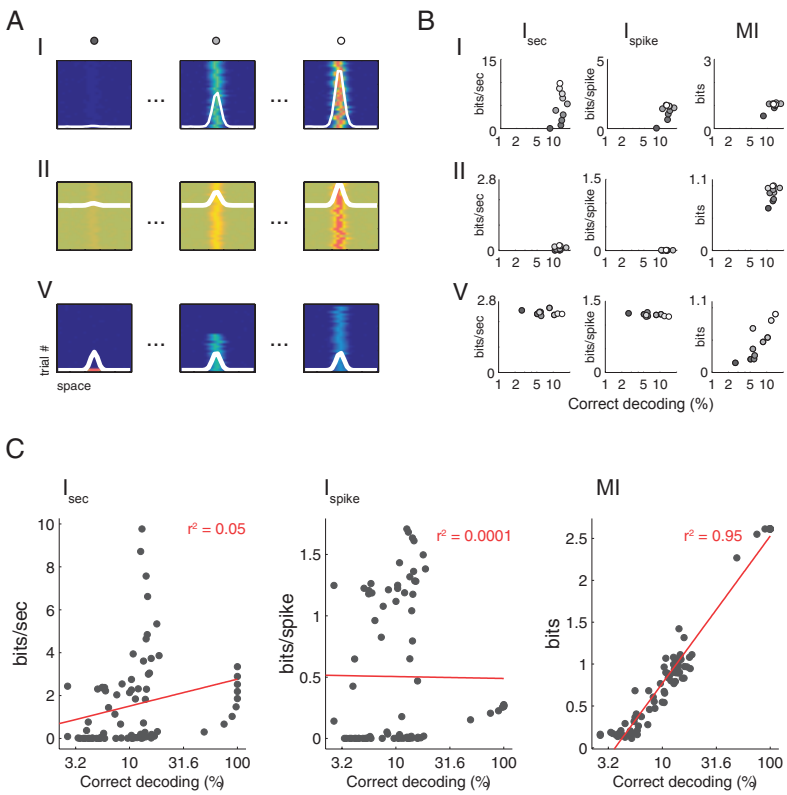

Figure 3. Assessing the performance of spatial information metrics. A. Examples of cell types I, II and V during three modulation conditions. Circles on top indicate the strength of spatial modulation, from black (low) to white (high). **B.** I_{sec}, I_{spike} and MI values of the cell types in A plotted against the percentage of correct decoding of the animal position (see Methods). Note that the same level of decoding across different cell types can elicit distinct I_{sec} and I_{spike} values (i.e. compare rows), and that similar values of I_{sec} or I_{spike} within a same cell type may be associated to different decoding levels (i.e., cell type V). **C.** Percentage of correct decoding for all simulated cells vs. I_{sec}, I_{spike} and MI along with the linear fit (red line). The MI best fits the percentage of correct decoding.

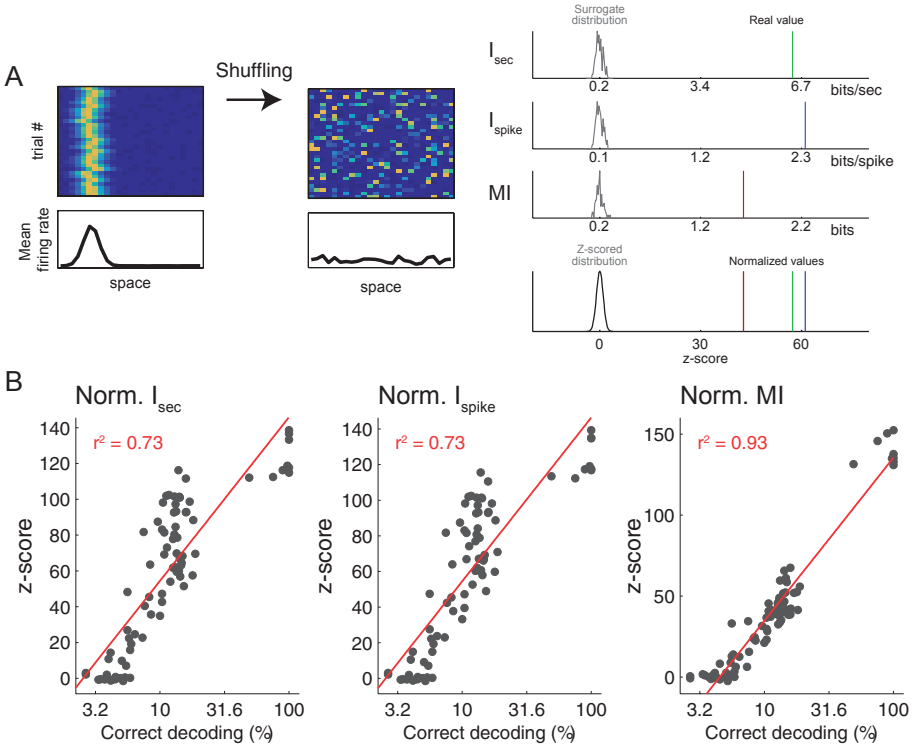

Figure 4. Correcting spatial metrics using surrogates. A. (Left) Example of shuffling procedure. To estimate chance information levels, the firing rate bins within trials were shuffled prior to computing the metrics. (Right) The actual value of each metric was compared to the surrogate distribution (n=100 shufflings) and z-score normalized. **B.** Percentage of correct decoding vs. the normalized values of I_{sec}, I_{spike} and MI for all simulated cells along with the linear fit (red line). Normalizing I_{sec} and I_{spike} significantly improves their correlation with decoding performance.

3B). Moreover, there were also cases in which I_{sec} and I_{spike} were insensitive to changes in the percentage of correct decoding (see V in Figure 3B). Across all the simulated cells, we found a clear correlation between decoding performance and MI, but not between correct decoding and either I_{sec} or I_{spike} (Figure 3C).

We next corrected the spatial information metrics for the chance information level of each cell, which varies according to firing characteristics. To that end, we computed information in shuffled rate-position maps to build a surrogate distribution of information values (Figure 4A). The actual value was then compared to and z-scored in relation to the chance distribution. While the correlation between decoding performance and MI did not show major changes after the normalization, the correlation of I_{sec} and I_{spike} with decoding substantially improved and became similar across metrics (Figure 4B).

We tested this approach using spikes from real cells recorded from the rat hippocampus during traversals on a linear track. The original and normalized MI, I_{sec} and I_{spike}

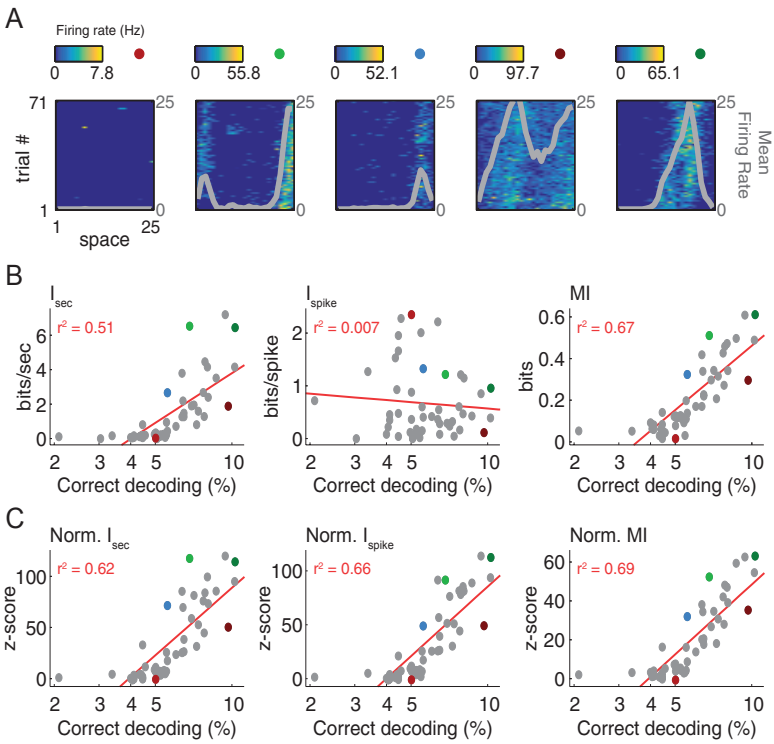

Figure 5. Spatial information metrics applied to real cell data. A. Example of the spatial activity of five neurons recorded in hippocampal CA1 of one rat during a linear track session. The recording included spatially modulated (i.e. place cells) as well as non-modulated cells. Colored circles mark the same cells highlighted in B and C. **B.** Scatter plots of information estimates and decoding performance for all recorded cells. Note that the MI exhibits the best correlation with decoding performance. **C.** Same as in B but for the normalized metrics. As in simulated data (Figure 3), normalizing I_{sec} and I_{spike} improves their correlation with decoding performance.

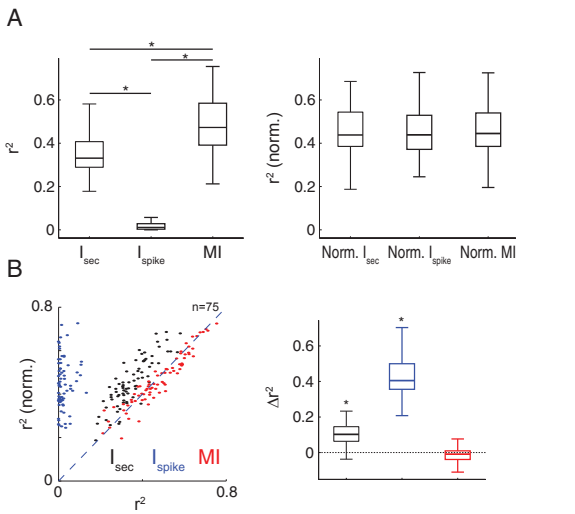

Figure 6. Correlation of spatial metrics and decoding performance. A. Boxplots show the distribution of coefficients of determination (r^2) between the percentage of correct decoding and I_{sec}, I_{spike} or MI for 75 linear track sessions. The original and normalized metrics are shown in the left and right panels, respectively. Notice similar r^2 values for the normalized metrics. *p<0.001 (Wilcoxon signed-rank tests, Bonferroni corrected). **B.** Scatter plot of the r^2 for each metric and its normalized version (left) and boxplots of the changes in r^2 after normalization (right). There is significant increase in r^2 for I_{sec} and I_{spike}; *p<0.001 (Wilcoxon signed-rank test, Bonferroni corrected).

were computed for each cell, and plotted against decoding performance. Figure 5 shows results for an example session. Notice in Figure 5B that the MI values correlated well with decoding performance, while I_{spike} showed no clear correlation (MI: r^2=0.67; I_{spike}: r^2=0.007). Unexpectedly, however, the I_{sec} values were better correlated to decoding than in our simulations (I_{sec}: r^2=0.51). The correlation with decoding substantially improved for I_{sec} and I_{spike} after the normalization, and reached similar values across all three metrics (Figure 5C). Figure 6A shows the r^2 values between each metric and decoding performance for 75 linear track sessions. Consistent with the example in Figure 5, we found that MI held the best correlations with decoding performance, followed by I_{sec}, while I_{spike} was poorly correlated. After normalization, the three metrics correlated similarly well with decoding. Figure 6B shows the changes in r^2 between the original and normalized versions of each metric. While the r^2 of I_{sec} and I_{spike} significantly increased, the r^2 changes for MI were not substantially different.

Discussion

We studied three metrics of spatial information using both simulated and real data. The performance of a Bayesian decoder was assumed to represent the gold standard of the true spatial information content of a cell. Decoders are used to predict the most likely stimulus that elicited a particular response; their performance is directly linked to the information about the stimulus contained in the response (Quian Quiroga and Panzeri, 2009). In other words, if two variables are related, it might be possible to use one of them to decode the other. The information contained in the confusion matrix of a decoder provides a lower bound to the information between the two variables (Quian Quiroga and Panzeri, 2009), allowing the use of decoding performance as an empirical estimate of the real (spatial) information of the cell (Huxter et al., 2008; Jensen and Lisman, 2000; Lopes-dos-Santos et al., 2015; Robertson et al., 1999). Under this framework, our results show that the mutual information (MI) better correlates with spatial decoding performance than I_{sec} and I_{spike}. Additionally, we found that the correlation with decoding performance achieves the same levels among the metrics following a surrogate-based normalization.

The low correlation of I_{sec} and I_{spike} with correct decoding in simulated data is a consequence of the way these metrics quantify information. Because they use the average firing rate over trials, a single trial with high firing rate can bias the metrics towards higher information values. This issue was apparent for simulated cells that were spatially modulated only in some of the trials (cell types IV and V): cells with different number of modulated trials but same mean firing rate showed similar information values (trial consistency; see Figure 7). This contrasts with the intuitive notion that the more consistent the spatial modulation of a cell across trials, the higher its spatial information. Another characteristic of I_{sec} and I_{spike} metrics was their sensitivity to changes in basal firing rate. We found that the same increase in firing rate but from different baseline levels (e.g., 0 to 5 Hz vs. 10 to 15 Hz) leads to different information values for I_{sec} and I_{spike}, favoring cells with low basal firing rate to have higher information (additive effect; Figure 7). Additionally, we found that the I_{sec} metric was sensitive to changes in the mean firing rate of a cell upon a multiplicative factor (multiplicative effect; Figure 7).

In contrast to I_{sec} and I_{spike}, the MI was able to capture the true spatial information of the cells irrespective of rate-position map features. For instance, in the example cases shown in Figure 3, the MI was capable of properly estimating the information despite differences in mean firing rate (cell types I and II). This is because the MI is based on the probability of each firing rate value and not on the value itself. In other words, as opposed to I_{sec} and I_{spike}, the MI is insensitive to additive and multiplicative effects (Figure 7). Moreover, the MI detected the increase of spatial information with higher trial consistency despite the constant mean firing rate across trials (cell type V). Notice that the MI takes into account the firing rate of every trial instead of the trial mean, making this metric more robust to inter-trial variability.

We introduced a normalization that estimates and corrects for the intrinsic bias present in the rate-position map. This bias is due to the fact that even shuffled firing rate maps will have information estimates above zero (i.e., random firing rate maps are seldom constant over space). After normalizing I_{sec} and I_{spike} by the mean and standard deviation of the shuffled distribution, we found an increase in their correlation with decoding performance, which reached the same level as the original MI (Figure 4). We found similar results when running our analyses on real linear-track data (Figures 5 and 6). Notably, I_{sec} had better

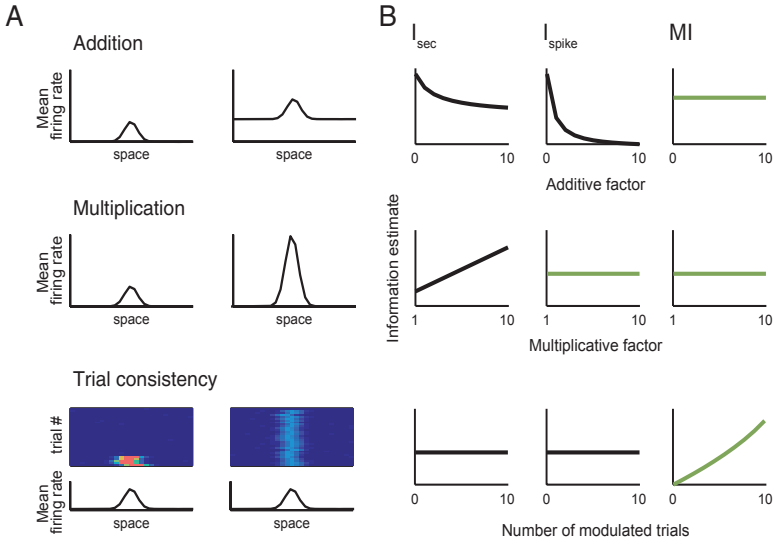

Figure 7. Influence of addition, multiplication and trial consistency on spatial metrics. A. Schematic examples of firing rate addition (top) and multiplication (middle), as well as of consistency over trials (bottom). In the latter case, the mean firing rate over trials was fixed. **B.** I_{sec}, I_{spike} and MI for different parameters of the cases in A. I_{sec} and I_{spike} decay as the additive factor increases, while I_{sec} linearly increases with the multiplication factor. Only the MI increases with trial consistency. The green curves are cases in which the metric behaves similarly to the decoding performance.

correlation with correct decoding in real than simulated data. This might be explained by the absence of some types of spatial modulation considered in our simulated cells, along with the expected presence of classical place cells in CA1 recordings.

These findings may have implications on what we know about spatial representations in the brain. For instance, previous studies measured spatial information in entorhinal cortex and hippocampus and found higher spatial information in putative excitatory than inhibitory neurons (Frank et al., 2001, 2000). However, this could reflect the bias of I_{spike} towards higher information values in cells with low mean firing rate (Figure 7B). More generally, our observations raise the question of what defines the spatial information of a neuron. For instance, most of the known correlates of space in the hippocampus focus on neurons that typically spike at very low rates outside their receptive fields (Fyhn et al., 2004; Hafting et al., 2005; O'Keefe and Dostrovsky, 1971; Taube et al., 1990). While I_{spike} and (mainly) I_{sec} work well to select cells with high spatial information in these cases, we wonder whether these metrics may have limited our understanding of spatial coding. In other words, the I_{sec} and I_{spike} are well suited to detect "canonical" place cells (i.e., cells whose spatial firing rate is a unimodal function centered on the place field), but may fail to detect other spatially informative neurons whose firing rate map is not that of a canonical place cell. Notice that adding a constant factor to a spatial firing rate map does not influence decoding performance nor the information estimated by the original MI, but decreases the amount of spatial information estimated by I_{sec} and I_{spike} (Figure 7). While some researchers may intuitively consider that cells which are silent outside the place field convey more information when they spike than cells with high basal firing rates, others may be more concerned as to whether it is possible or not to decode the animal position from the firing rate of the cell. The latter would further argue that every cell that carries information about the animal position (as retrieved by a decoder) could be called a "place cell", independently of place field shape or mean firing rate. Noteworthy, the existence of unconventional spatial representations has been recently demonstrated for medial entorhinal cortex neurons (Diehl et al., 2017; Hardcastle et al., 2017). In any case, irrespective of the diverging views, our results show that the MI and the corrections proposed here for I_{sec} and I_{spike} are suitable metrics to capture other types of less canonical spatial correlates that may have gone undetected so far.

Acknowledgements

This work was supported by CAPES and CNPq, Brazil. We thank the Buzsáki laboratory for making data publicly available at http://crcns.org/, a data-sharing website supported by NSF and NIH, USA. We thank D. Laplagne and R. Romcy-Pereira for critical discussions.

References

Diehl, G.W., Hon, O.J., Leutgeb, S., Leutgeb, J.K., 2017. Grid and Nongrid Cells in Medial Entorhinal Cortex Represent Spatial Location and Environmental Features with Complementary Coding Schemes. Neuron 94, 83–92.

Eichenbaum, H., 2000. A cortical–hippocampal system for declarative memory. Nat. Rev. Neurosci. 1, 41–50.

Frank, L.M., Brown, E.N., Wilson, M., 2000. Trajectory Encoding in the Hippocampus and Entorhinal Cortex. Neuron 27, 169–178.

Frank, L.M., Brown, E.N., Wilson, M.A., 2001. A comparison of the firing properties of putative excitatory and inhibitory neurons from CA1 and the entorhinal cortex. J. Neurophysiol. 86, 2029–2040.

Fyhn, M., Molden, S., Witter, M.P., Moser, E.I., Moser, M.-B., 2004. Spatial representation in the entorhinal cortex. Science 305, 1258–1264.

Hafting, T., Fyhn, M., Molden, S., Moser, M.-B., Moser, E.I., 2005. Microstructure of a spatial map in the entorhinal cortex. Nature 436, 801–806.

Hardcastle, K., Maheswaranathan, N., Ganguli, S., Giocomo, L.M., 2017. A Multiplexed, Heterogeneous, and Adaptive Code for Navigation in Medial Entorhinal Cortex. Neuron 94, 375–387.

Huxter, J., Burgess, N., O'Keefe, J., 2003. Independent rate and temporal coding in hippocampal pyramidal cells. Nature 425, 828–832.

Huxter, J.R., Senior, T.J., Allen, K., Csicsvari, J., 2008. Theta phase–specific codes for two-dimensional position, trajectory and heading in the hippocampus. Nat. Neurosci. 11, 587–594.

Jensen, O., Lisman, J.E., 2000. Position reconstruction from an ensemble of hippocampal place cells: contribution of theta phase coding. J. Neurophysiol. 83, 2602–2609.

Kropff, E., Carmichael, J.E., Moser, M.-B., Moser, E.I., 2015. Speed cells in the medial entorhinal cortex. Nature 523, 419.

Lopes-dos-Santos, V., Panzeri, S., Kayser, C., Diamond, M.E., Quian Quiroga, R., 2015. Extracting information in spike time patterns with wavelets and information theory. J. Neurophysiol. 113, 1015–1033.

Mizuseki, K., Sirota, A., Pastalkova, E., Diba, K., Buzsáki, G., 2013. Multiple single unit recordings from different rat hippocampal and entorhinal regions while the animals were performing multiple behavioral tasks. CRCNS Org.

Morris, R.G.M., Garrud, P., Rawlins, J.N.P., O'Keefe, J., 1982. Place navigation impaired in rats with hippocampal lesions. Nature 297, 681–683.

Moser, E.I., Kropff, E., Moser, M.-B., 2008. Place cells, grid cells, and the brain's spatial representation system. Annu Rev Neurosci 31, 69–89.

O'Keefe, J., Dostrovsky, J., 1971. The hippocampus as a spatial map. Preliminary evidence from unit activity in the freely-moving rat. Brain Res. 34, 171–175.

O'Keefe, J., Recce, M.L., 1993. Phase relationship between hippocampal place units and the EEG theta rhythm. Hippocampus 3, 317–330.

Quian Quiroga, R., Panzeri, S., 2009. Extracting information from neuronal populations: information theory and decoding approaches. Nat. Rev. Neurosci. 10, 173–185.

Robertson, R.G., Rolls, E.T., Georges-François, P., Panzeri, S., others, 1999. Head direction cells in the primate pre-subiculum. Hippocampus 9, 206–219.

Scoville, W.B., Milner, B., 1957. Loss of recent memory after bilateral hippocampal lesions. J. Neurol. Neurosurg. Psychiatry 20, 11.

Shannon, C.E., 1948. A mathematical theory of communication, Part I, Part II. Bell Syst Tech J 27, 623–656.

Skaggs, W.E., McNaughton, B.L., Gothard, K.M., Markus, E.J., 1993. An information-theoretic approach to deciphering the hippocampal code, in: Advances in Neural Information Processing Systems 5. eds. Hanson, S.J., Giles, C.L. & Cowan, J.D., pp. 1030–1037.

Skaggs, W.E., McNaughton, B.L., Wilson, M.A., Barnes, C.A., 1996. Theta phase precession in hippocampal neuronal populations and the compression of temporal sequences. Hippocampus 6, 149–172.

Souza, B.C., Tort, A.B.L., 2017. Asymmetry of the temporal code for space by hippocampal place cells. Sci. Rep. 7.

Taube, J.S., Muller, R.U., Ranck, J.B., 1990. Head-direction cells recorded from the postsubiculum in freely moving rats. I. Description and quantitative analysis. J. Neurosci. 10, 420–435.

Vanderwolf, C.H., 1969. Hippocampal electrical activity and voluntary movement in the rat. Electroencephalogr. Clin. Neurophysiol. 26, 407–418.

Zola-Morgan, S.M., Squire, L.R., 1990. The primate hippocampal formation: evidence for a time-limited role in memory storage. Science 250, 288–290.